

# Performance of Multi-Antenna Signaling Techniques in the Presence of Polarization Diversity

R. U. Nabar, H. Bölcskei, V. Erceg, D. Gesbert, and A. J. Paulraj

**Abstract** – Multiple-input multiple-output (MIMO) antenna systems employ *spatial multiplexing* to increase spectral efficiency or *transmit diversity* to improve link reliability. The performance of these signaling strategies is highly dependent on MIMO channel characteristics which in turn depend on antenna height and spacing and richness of scattering. In practice, large antenna spacings are often required to achieve significant multiplexing or diversity gains. The use of dual-polarized antennas (*polarization diversity*) is a promising cost- and space-effective alternative where two spatially separated uni-polarized antennas are replaced by a single antenna structure employing orthogonal polarizations. This paper investigates the performance of spatial multiplexing and transmit diversity (Alamouti scheme) in MIMO wireless systems employing dual-polarized antennas. In particular, we derive estimates for the uncoded average symbol error rate of spatial multiplexing and transmit diversity and identify channel conditions where the use of polarization diversity yields performance improvements. We show that while improvements in terms of symbol error rate of up to an order of magnitude are possible in the case of spatial multiplexing, the presence of polarization diversity generally incurs a performance loss for transmit diversity techniques. Finally, we provide simulation results to demonstrate that our estimates closely match the actual symbol error rates.

**Keywords:** MIMO, polarization diversity, spatial multiplexing, transmit diversity, Alamouti scheme

**Topic Area:** Capacity and Performance Limits

\*Submitted to *IEEE Trans. Signal Processing*, Aug. 2001, revised, Feb. 2002, final version May 2002.

R. U. Nabar and A. J. Paulraj are with the Information Systems Laboratory, Stanford University, Stanford, CA. Address: 228 Packard, 350 Serra Mall, Stanford, CA 94305, USA. Phone: (650)-725-6099 Fax: (650)-723-8473, E-mail: {nabar, apaulraj}@stanford.edu

H. Bölcskei is with the Communication Technology Laboratory, Swiss Federal Institute of Technology (ETH), Zurich, Switzerland. E-mail: boelcskei@nari.ee.ethz.ch

V. Erceg is with Iospan Wireless Inc., San Jose, CA, USA. E-mail: verceg@iospanwireless.com

D. Gesbert is with the Department of Informatics, University of Oslo, Norway. E-mail: gesbert@ifi.uio.no

## I. INTRODUCTION AND OUTLINE

The use of multiple antennas at both ends of a wireless link (MIMO technology) has recently been shown to have the potential to drastically increase spectral efficiency through a technique known as *spatial multiplexing (SM)* [1]-[5]. This leverage often referred to as multiplexing gain permits the opening of multiple spatial data pipes between transmitter and receiver within the frequency band of operation for no additional power expenditure, leading to a linear (in the number of antennas) increase in capacity. Multiple antennas at both ends of a wireless link can also be used to improve link reliability through the use of *transmit diversity (TD)* techniques. TD techniques such as space-time coding [6]-[10] are particularly attractive since they do not require channel knowledge in the transmitter. The resulting diversity gain improves the reliability of fading wireless links and hence results in improved quality of transmission.

The performance of SM and TD depends strongly on the overall MIMO channel which in turn is a function of transmit and receive antenna characteristics such as height and spacing and the scattering environment. In general, antenna spacings of tens of wavelengths at the base-station and up to a wavelength at the subscriber unit are required in order to achieve significant multiplexing or diversity gains. Unfortunately, large antenna spacing increases both size and cost of base stations and renders the use of multiple antennas in handsets very difficult. The use of dual-polarized antennas is a promising cost- and space-effective alternative where two spatially separated uni-polarized antennas are replaced by a single antenna structure employing two orthogonal polarizations.

**Contributions.** In this paper, we investigate the performance of uncoded SM and TD (in particular the Alamouti scheme [10]), in systems employing dual-polarized antennas. Although our techniques are generally applicable, for the sake of simplicity and clarity of exposition, we consider a link with one dual-polarized transmit and one dual-polarized receive antenna. Our contributions are as follows.

- We introduce a *channel model* for wireless links employing dual-polarized antennas taking into account cross-polarization discrimination (XPD), Ricean K-factor, and fading signal correlation.
- We propose a new method for *computing estimates of the uncoded average symbol error rate* of SM and the Alamouti scheme in the presence of polarization diversity.
- We *identify channel conditions* where the use of *polarization diversity is beneficial* from an

error-probability point of view, and we show that improvements in terms of symbol error rate of up to an order of magnitude are possible depending on the transmission scheme.

- We demonstrate that our *symbol error rate estimates closely match the actual error rates*. Our method can therefore be used to *predict performance trends* analytically and helps avoid time-consuming computer simulations.

**Organization of the paper.** The rest of this paper is organized as follows. Section II introduces the channel model and states our assumptions. In Sections III and IV, we derive estimates for the uncoded average symbol error rate of SM and the Alamouti scheme, respectively, as a function of the propagation parameters. Section V provides simulation results and demonstrates that our estimates closely match the simulation results. Finally, Section VI contains our conclusions.

## II. THE CHANNEL MODEL

We consider a system with one dual-polarized transmit and one dual-polarized receive antenna. The channel is assumed to be frequency-flat over the band of interest. A channel model for this antenna configuration for the Rayleigh fading case was first introduced by the authors in [11]. Guided by insights gained through the measurement results reported in [12], we extend this channel model to include Ricean fading as well. We have the following input-output relation<sup>1</sup>

$$\mathbf{r} = \sqrt{E_s} \mathbf{H} \mathbf{x} + \mathbf{n},$$

where

- $\mathbf{x} = [x_0 \ x_1]^T$  is the  $2 \times 1$  transmit signal vector (also called codevector) whose elements are taken from a finite (complex) constellation chosen such that the average energy of the constellation elements is 1

- $\mathbf{r} = [r_0 \ r_1]^T$  is the  $2 \times 1$  received signal vector

- $\mathbf{n}$  is the  $2 \times 1$  temporally i.i.d. zero-mean complex gaussian noise vector satisfying  $\mathcal{E}\{\mathbf{n}\mathbf{n}^H\} = \sigma_n^2 \mathbf{I}_2$

- $\mathbf{H} = \begin{bmatrix} h_{0,0} & h_{0,1} \\ h_{1,0} & h_{1,1} \end{bmatrix}$  is the  $2 \times 2$  channel transfer matrix or polarization matrix

<sup>1</sup>The superscripts  $T$  and  $H$  stand for transpose and conjugate transpose, respectively.  $\mathcal{E}$  is the expectation operator and  $\mathbf{I}_m$  is the identity matrix of dimension  $m \times m$ .

- $E_s$  is the average energy available at each of the transmit antennas over a symbol period.

The polarization matrix  $\mathbf{H}$  describes the degree of suppression of individual co-and cross-polarized components, cross-correlation, and cross-coupling of energy from one polarization state to the other polarization state. In practice, two polarization schemes are typically used: *horizontal/vertical* ( $0^\circ/90^\circ$ ) or *slanted* ( $+45^\circ/-45^\circ$ ). In this paper, we assume that both transmitter and receiver employ the same polarization scheme, i.e., both of them employ either  $+45^\circ/-45^\circ$  (see Fig. 1) or  $0^\circ/90^\circ$ . The signals  $x_0$  and  $x_1$  are transmitted on the two different polarizations, and  $r_0$  and  $r_1$  are the signals received on the corresponding polarizations. We emphasize that although we are dealing with one physical transmit and one physical receive antenna, the underlying channel is a 2-input 2-output channel, since each polarization mode is treated as a separate physical channel. The elements of  $\mathbf{H}$  are (in general correlated) complex gaussian random variables. We decompose the channel matrix into the sum of an average (or fixed, possibly line-of-sight) component and a variable (or scattered) component as follows

$$\mathbf{H} = \sqrt{\frac{K}{1+K}} \overline{\mathbf{H}} + \sqrt{\frac{1}{1+K}} \widetilde{\mathbf{H}}, \quad (1)$$

where  $\mathcal{E}\{\mathbf{H}\} = \sqrt{\frac{K}{1+K}} \overline{\mathbf{H}}$  and  $\sqrt{\frac{1}{1+K}} \widetilde{\mathbf{H}}$  are the average and variable components of the channel matrix, respectively. The factors  $\sqrt{\frac{K}{1+K}}$  and  $\sqrt{\frac{1}{1+K}}$  in (1) are energy normalization factors and are related to the Ricean K-factor as will be described later in this section. The elements of the matrix  $\widetilde{\mathbf{H}}$ , denoted as  $\widetilde{h}_{i,j}$  ( $i, j = 0, 1$ ), are zero-mean circularly symmetric complex gaussian random variables whose variances depend on the propagation conditions and the antenna characteristics. Throughout this paper, we set

$$\begin{aligned} \mathcal{E}\{|\widetilde{h}_{0,0}|^2\} &= \mathcal{E}\{|\widetilde{h}_{1,1}|^2\} = 1 \\ \mathcal{E}\{|\widetilde{h}_{0,1}|^2\} &= \mathcal{E}\{|\widetilde{h}_{1,0}|^2\} = \alpha, \end{aligned}$$

where  $0 < \alpha \leq 1$  is directly related to the XPD (or separation of orthogonal polarizations) for the variable component of the channel. Good discrimination of orthogonal polarizations amounts to small values of  $\alpha$  and vice versa. We note that  $\alpha$  is not only a function of the antenna elements' ability to separate orthogonal polarizations but also of the propagation environment (coupling between orthogonal polarizations due to scattering). Measurements conducted in the 2.5 GHz band [13] have shown that even if antennas with good XPD are used scattering in the propagation environment changes the polarization states and hence  $\alpha$  which describes the joint

effect of antenna characteristics and the channel may be close to 1. In particular, it was found in [13] that for ranges beyond 1.6 km  $\alpha$  is always close to 1. The elements of the matrix  $\overline{\mathbf{H}}$ , denoted as  $\overline{h}_{i,j}$  ( $i, j = 0, 1$ ), do not vary and are complex numbers satisfying

$$|\overline{h}_{0,0}|^2 = |\overline{h}_{1,1}|^2 = 1, \quad |\overline{h}_{0,1}|^2 = |\overline{h}_{1,0}|^2 = \alpha_f,$$

where  $0 \leq \alpha_f \leq 1$  is directly related to the XPD for the fixed component of the channel. It is important to note that the presence of a fixed channel component does not always imply line-of-sight conditions. For pure line-of-sight conditions  $\alpha_f$  unlike  $\alpha$  is solely a function of the antennas' ability to separate the orthogonal polarizations.

The Ricean K-factor for a fading channel is generally defined as the ratio of the power in the fixed component to the power in the variable component [14]. Under the assumptions made above, the K-factor for each element of the channel matrix,  $K_{i,j}$  ( $i, j = 0, 1$ ), can be expressed as follows

$$K_{0,0} = K_{1,1} = K, \quad K_{0,1} = K_{1,0} = \frac{\alpha_f}{\alpha} K.$$

For the remainder of this paper, we shall refer to  $K$  as the K-factor of the channel. Note that  $K = 0$  corresponds to the case of pure Rayleigh fading. Experimental data collected in [12], [13] reveals that the elements of  $\mathbf{H}$  are in general correlated. We therefore define the following correlation coefficients<sup>2</sup>

$$\begin{aligned} t &= \frac{\mathcal{E}\{\tilde{h}_{0,0} \tilde{h}_{0,1}^*\}}{\sqrt{\alpha}} = \frac{\mathcal{E}\{\tilde{h}_{1,0} \tilde{h}_{1,1}^*\}}{\sqrt{\alpha}} \\ r &= \frac{\mathcal{E}\{\tilde{h}_{0,0} \tilde{h}_{1,0}^*\}}{\sqrt{\alpha}} = \frac{\mathcal{E}\{\tilde{h}_{0,1} \tilde{h}_{1,1}^*\}}{\sqrt{\alpha}}, \end{aligned}$$

where  $t$  is referred to as the transmit correlation coefficient and  $r$  is the receive correlation coefficient. Recall that we assumed that  $\alpha > 0$ , which ensures viability of the above definitions. Experimental data also reveals that the correlation between the diagonal elements of the channel matrix,  $\tilde{h}_{0,0}$  and  $\tilde{h}_{1,1}$ , and the off-diagonal elements,  $\tilde{h}_{0,1}$  and  $\tilde{h}_{1,0}$ , is typically very small. For the sake of simplicity, throughout the paper, we therefore assume that  $\mathcal{E}\{\tilde{h}_{0,0} \tilde{h}_{1,1}^*\} = \mathcal{E}\{\tilde{h}_{1,0} \tilde{h}_{0,1}^*\} = 0$ . Measured values of XPD, K-factor, and correlation coefficients can be found in [13], [15], [16], [17], [18].

We conclude this section by noting that the above assumptions on the propagation conditions lead to a certain symmetry in the channel model, simplifying the ensuing analysis, and better

<sup>2</sup>The superscript \* stands for complex conjugate.

describe the case where the signals are launched and received on orthogonal polarizations of  $\pm 45^\circ$ . This is due to the symmetry in reflections off the earth's surface for both polarizations, which is not the case for other polarization configurations such as  $0^\circ/90^\circ$ . We shall therefore focus on the  $\pm 45^\circ$  polarization configuration (see Fig. 1) for the remainder of this paper, keeping in mind, however, that the techniques presented are more generally applicable (with slight modifications of the channel model).

### III. SYMBOL ERROR RATE ESTIMATE FOR SPATIAL MULTIPLEXING

In this section, we first briefly review spatial multiplexing (SM), and then present a new method for estimating the average (over the random channel) uncoded symbol error rate of SM as a function of the propagation parameters.

**Spatial Multiplexing.** Multiple antenna systems employ SM [1]-[5] to increase spectral efficiency. Fig. 2 shows a schematic of SM for the dual-polarized antenna system under consideration. The symbol stream to be transmitted is divided into two sub-streams, which are then launched simultaneously from the two orthogonal polarizations. We assume that the receiver has perfect channel knowledge and performs maximum-likelihood (ML) detection.

**Average Symbol Error Rate Estimate.** Assuming perfect channel state information, the ML decoder computes the vector  $\hat{\mathbf{x}}$  according to

$$\hat{\mathbf{x}} = \arg \min_{\mathbf{x}} \left\| \mathbf{r} - \sqrt{E_s} \mathbf{H} \mathbf{x} \right\|^2,$$

where the minimization is performed over the set of all possible codevectors  $\mathbf{x}$ . Let  $\mathbf{f} = [f_0 \ f_1]^T$  and  $\mathbf{g} = [g_0 \ g_1]^T$  be two different codevectors of size  $2 \times 1$  and assume that  $\mathbf{f}$  was transmitted. For a given channel realization  $\mathbf{H}$ , the probability that the receiver decides erroneously in favor of the vector  $\mathbf{g}$  is given by [19]

$$P(\epsilon | \mathbf{H}) = Q \left( \sqrt{\frac{E_s}{2\sigma_n^2}} d^2(\epsilon | \mathbf{H}) \right), \quad (2)$$

where  $d^2(\epsilon | \mathbf{H}) = \|\mathbf{H}\epsilon\|^2$  with the vector error event  $\epsilon = \mathbf{f} - \mathbf{g} = [\epsilon_0 \ \epsilon_1]^T$ . Upon defining  $\mathbf{y} = \mathbf{H}\epsilon$ , we get  $d^2(\epsilon | \mathbf{H}) = \|\mathbf{y}\|^2$  and using the Chernoff bound  $Q(x) \leq e^{-\frac{x^2}{2}}$ , it follows from (2) that

$$P(\epsilon | \mathbf{H}) \leq e^{-\frac{E_s}{4\sigma_n^2} \|\mathbf{y}\|^2}. \quad (3)$$

Since  $\mathbf{H}$  was assumed to be complex gaussian it follows that the  $2 \times 1$  vector  $\mathbf{y}$  is complex gaussian as well. Furthermore, using (1) the vector  $\mathbf{y}$  can be decomposed into a deterministic component  $\bar{\mathbf{y}}$  and a fading component  $\tilde{\mathbf{y}}$  as follows

$$\begin{aligned}\bar{\mathbf{y}} &= \sqrt{\frac{K}{1+K}} \bar{\mathbf{H}} \boldsymbol{\epsilon} \\ \tilde{\mathbf{y}} &= \sqrt{\frac{1}{1+K}} \tilde{\mathbf{H}} \boldsymbol{\epsilon}.\end{aligned}$$

The average over all channel realizations of the RHS in (3) is fully characterized by the eigenvalues of the  $2 \times 2$  covariance matrix  $\mathbf{C}_{\tilde{\mathbf{y}}} = \mathcal{E}\{\tilde{\mathbf{y}} \tilde{\mathbf{y}}^H\} = \mathbf{U} \boldsymbol{\Lambda} \mathbf{U}^H$  where  $\boldsymbol{\Lambda} = \text{diag}\{\lambda_i\}_{i=0}^1$ , and the fixed component  $\bar{\mathbf{y}}$  [20]. Specifically,<sup>3</sup>

$$P(\boldsymbol{\epsilon}) \leq e^{-\frac{E_s}{4\sigma_n^2} \|\bar{\mathbf{y}}\|^2} \prod_{i=0}^{\text{r}(\mathbf{C}_{\tilde{\mathbf{y}}})-1} \frac{e^{-\frac{\left(\frac{E_s}{4\sigma_n^2} |d_i| \lambda_i\right)^2}{1 + \frac{E_s}{4\sigma_n^2} \lambda_i}}}{1 + \frac{E_s}{4\sigma_n^2} \lambda_i}, \quad (4)$$

where  $P(\boldsymbol{\epsilon}) = \mathcal{E}_{\mathbf{H}}\{P(\boldsymbol{\epsilon}|\mathbf{H})\}$  is the pairwise error probability (PEP) averaged over all channel realizations and

$$\mathbf{d} = [d_0 \ d_1]^T = \begin{bmatrix} \frac{1}{\sqrt{\lambda_0}} & 0 \\ 0 & \frac{1}{\sqrt{\lambda_1}} \end{bmatrix} \mathbf{U}^H \bar{\mathbf{y}},$$

in the case of full-rank  $\mathbf{C}_{\tilde{\mathbf{y}}}$  and

$$d_0 = \left[ \frac{1}{\sqrt{\lambda_0}} \ 0 \right] \mathbf{U}^H \bar{\mathbf{y}}, \quad d_1 = 0,$$

in the case of rank-deficient  $\mathbf{C}_{\tilde{\mathbf{y}}}$ . We remark that in the absence of a fixed component (pure Rayleigh fading)  $\bar{\mathbf{y}} = \mathbf{0}$  and hence  $d_0 = d_1 = 0$  which implies  $P(\boldsymbol{\epsilon}) \leq \prod_{i=0}^{\text{r}(\mathbf{C}_{\tilde{\mathbf{y}}})-1} \frac{1}{1 + \frac{E_s}{4\sigma_n^2} \lambda_i}$ .

Furthermore, we note that (4) includes the results for the correlated Rayleigh fading case reported in [21], [22], [23] and the results for the case of independent Ricean fading in [8] as special cases. Straightforward manipulations reveal that<sup>4</sup>

$$\mathbf{C}_{\tilde{\mathbf{y}}} = \frac{1}{1+K} \begin{bmatrix} a & b \\ b^* & d \end{bmatrix},$$

<sup>3</sup> $\text{r}(\mathbf{A})$  stands for the rank of the matrix  $\mathbf{A}$ .

<sup>4</sup> $\Re(x)$  stands for the real part of  $x$ .

where

$$\begin{aligned} a &= |\epsilon_0|^2 + \alpha|\epsilon_1|^2 + 2\Re\{\epsilon_0\epsilon_1^*t\sqrt{\alpha}\} \\ b &= r\sqrt{\alpha}(|\epsilon_0|^2 + |\epsilon_1|^2) \\ d &= \alpha|\epsilon_0|^2 + |\epsilon_1|^2 + 2\Re\{\epsilon_0\epsilon_1^*t\sqrt{\alpha}\}, \end{aligned}$$

and the eigenvalues of  $\mathbf{C}_{\tilde{\mathbf{y}}}$  are given by

$$\lambda_{0,1} = \frac{a + d \pm \sqrt{(a - d)^2 + 4|b|^2}}{2(1 + K)}.$$

From the expressions developed so far, it is interesting to note that transmit and receive correlation have asymmetric impacts on the probability of error associated with a particular error event. We shall refer to this observation in Sec. V.

Consider a situation where no polarization diversity is used (i.e.  $\alpha = 1$ ) and the channel matrix is i.i.d. with pure Rayleigh fading ( $K = 0$ ). In this case  $\lambda_0 = \lambda_1 = |\epsilon_0|^2 + |\epsilon_1|^2$  and the error rate behavior is governed by error events where only one out of the two scalar symbols is in error, say  $\epsilon_0 \neq 0$  with  $|\epsilon_0|^2 = d_{min}^2$  where  $d_{min}$  denotes the minimum Euclidean distance of the (complex) scalar constellation used. Clearly, the error rate will decay for increasing  $d_{min}$ . In the general case the error events governing the performance of SM exhibit significant dependence on the channel geometry induced by the channel statistics. In order to avoid having to find those error events for a particular channel geometry, we average over all possible error events including a weighting which takes into account that different vector error events cause a different number of scalar symbol errors. It is important to note that different vector error events have potentially different frequencies of occurrence and that this must be accounted for in the averaging. To capture this effect we find the relative frequencies of the various error events by enumerating all possible codeword difference vectors<sup>5</sup>  $\boldsymbol{\epsilon} \neq \mathbf{0}$  and calculating the percentage of occurrence of each vector error event. We shall refer to the  $i$ -th element of the set of vector error events as  $\boldsymbol{\epsilon}_i = [\epsilon_{i,0} \ \epsilon_{i,1}]^T$ .

For the remainder of this section, we shall consider the case of 4-QAM transmission, where the individual scalar error events  $\epsilon_{i,k}$  ( $k = 0, 1$ ) can take values from the set  $\{0, \pm d_{min}, \pm j d_{min}, \pm d_{min}(1 + j), \pm d_{min}(1 - j)\}$ . Now, the relative frequency of an error event  $\boldsymbol{\epsilon}_i$ , denoted as  $n(\boldsymbol{\epsilon}_i)$ ,

<sup>5</sup> $\mathbf{0}$  stands for the all zeros matrix of appropriate dimension.

is given by

$$n(\boldsymbol{\epsilon}_i) = \frac{\omega(\epsilon_{i,0})\omega(\epsilon_{i,1})}{240}$$

with

$$\omega(x) = \begin{cases} 4, & x = 0 \\ 2, & x = \pm d_{min}, \pm jd_{min} \\ 1, & \pm d_{min}(1+j), \pm d_{min}(1-j). \end{cases}$$

We also define a function  $s(\boldsymbol{\epsilon}_i)$  which reflects the number of scalar symbol errors that the error event  $\boldsymbol{\epsilon}_i$  is associated with. In particular, we have

$$s(\boldsymbol{\epsilon}_i) = \begin{cases} 2, & \epsilon_{i,0} \neq 0 \text{ and } \epsilon_{i,1} \neq 0 \\ 1, & \epsilon_{i,0} = 0 \text{ or } \epsilon_{i,1} = 0. \end{cases}$$

We can now estimate the average symbol error rate of spatial multiplexing as

$$\bar{P}_{mux} \approx \sum_{\boldsymbol{\epsilon}_i} n(\boldsymbol{\epsilon}_i)P(\boldsymbol{\epsilon}_i)s(\boldsymbol{\epsilon}_i), \quad (5)$$

where  $P(\boldsymbol{\epsilon}_i)$  is the RHS of (4). In Sec. V,  $\bar{P}_{mux}$  is shown to reveal the correct performance trends with varying channel statistics and a close match between the exact symbol error rate and  $\bar{P}_{mux}$  is found.

We note that in some cases (4) and (5) can be used to study the impact of channel statistics on the uncoded symbol error rate analytically. For example, it follows immediately from (4) and (5) that for  $t = r = 0$  and pure Rayleigh fading ( $K = 0$ ), the quantity  $\bar{P}_{mux}$  will be minimum for  $\alpha = 1$ , i.e., for the case where no polarization diversity is employed. Indeed, we will find in Sec. V (Simulation Examples 2 and 3) that for pure Rayleigh fading, polarization diversity improves the multiplexing gain only in the presence of high fading signal correlation. We will furthermore see that in the Ricean case the use of polarization diversity can improve the performance of SM significantly.

#### IV. SYMBOL ERROR RATE ESTIMATE FOR TRANSMIT DIVERSITY

In this section, we shall briefly review the Alamouti scheme, and then present the corresponding uncoded symbol error rate estimate as a function of the channel statistics.

**Alamouti Scheme.** TD schemes exploit spatial diversity inherent in MIMO systems to improve link reliability. We consider the performance of a simple TD scheme, the Alamouti

scheme [10], for the polarization diversity channel under consideration. A schematic of the transmission strategy for the Alamouti scheme is shown in Fig. 3. Unlike SM, TD schemes introduce redundancy in the transmitted symbol stream to exploit spatial diversity. Thus, if symbols  $s_0$  and  $s_1$  are transmitted at  $+45^\circ$  and  $-45^\circ$ , respectively, during one symbol period, then during the following symbol period, symbols  $-s_1^*$  and  $s_0^*$  are launched at  $+45^\circ$  and  $-45^\circ$ , respectively. We assume that the channel remains constant over at least two symbol periods and that the receiver performs ML detection on the received signals. As for the case of SM, we assume that the receiver maintains perfect channel knowledge.

**Average Symbol Error Rate for the Alamouti Scheme.** The ML receiver for the Alamouti scheme is much simpler than that for SM. This is due to the fact that the structure of the transmitted signal orthogonalizes the channel irrespectively of the channel realization. Appropriate processing at the receiver effectively collapses the vector detection problem into simpler scalar detection problems. Denoting the squared Frobenius norm<sup>6</sup> of the channel matrix  $\mathbf{H}$  by  $\|\mathbf{H}\|_F^2$ , the input-output relation for the Alamouti scheme for either of the transmitted scalar symbols,  $s_0$  or  $s_1$ , is given by [10]

$$\tilde{r}_i = \sqrt{E_s} \|\mathbf{H}\|_F^2 s_i + \tilde{n}_i, \quad i = 0, 1,$$

where  $\tilde{r}_i$  is the scalar processed received signal corresponding to transmitted symbol  $s_i$  ( $i = 0, 1$ ) and  $\tilde{n}_i$  is scalar zero-mean complex gaussian noise with variance  $\mathcal{E}\{|\tilde{n}_i|^2\} = \|\mathbf{H}\|_F^2 \sigma_n^2$ . Standard scalar ML detection can be performed on  $\tilde{r}_i$  according to

$$\hat{s}_i = \arg \min_{s_i} |\tilde{r}_i - \sqrt{E_s} \|\mathbf{H}\|_F^2 s_i|^2,$$

where  $\hat{s}_i$  is the estimated data symbol and the minimization is performed over all possible scalar constellation points. Assuming that  $s_i$  is taken from a QAM constellation, the probability that the receiver decodes the transmitted symbol in error for a given channel realization may be approximated by [24]

$$P(\hat{s}_i \neq s_i | \mathbf{H}) \approx \bar{N}_e Q \left( \sqrt{d_{min}^2 \frac{E_s \|\mathbf{H}\|_F^2}{2\sigma_n^2}} \right), \quad (6)$$

where  $\bar{N}_e$  and  $d_{min}$  are the average number of nearest neighbors and minimum distance of the underlying QAM constellation, respectively. Again, using the Chernoff bound we can upper-

<sup>6</sup>The squared Frobenius norm of a matrix  $\mathbf{A}$  is given by  $\|\mathbf{A}\|_F^2 = \text{Tr}(\mathbf{A}\mathbf{A}^H)$ , where  $\text{Tr}$  is the trace operator.

bound the RHS of (6) as

$$P(\hat{s}_i \neq s_i | \mathbf{H}) \leq \bar{N}_e e^{-\frac{E_s d_{min}^2}{4\sigma_n^2} \|\mathbf{y}\|^2}, \quad (7)$$

where<sup>7</sup>  $\mathbf{y} = \text{vec}(\mathbf{H})$ . As for the case of SM, the vector  $\mathbf{y}$  can be decomposed into a fixed component  $\bar{\mathbf{y}}$  and a variable component  $\tilde{\mathbf{y}}$  as follows

$$\begin{aligned} \bar{\mathbf{y}} &= \text{vec} \left( \sqrt{\frac{K}{1+K}} \bar{\mathbf{H}} \right) \\ \tilde{\mathbf{y}} &= \text{vec} \left( \sqrt{\frac{1}{1+K}} \tilde{\mathbf{H}} \right). \end{aligned}$$

Again, since  $\mathbf{H}$  is complex gaussian the vector  $\mathbf{y}$  is also complex gaussian and the RHS of (7) averaged over all channel realizations is completely characterized by the eigenvalues of the  $4 \times 4$  covariance matrix  $\mathbf{C}_{\tilde{\mathbf{y}}} = \mathcal{E}\{\tilde{\mathbf{y}}\tilde{\mathbf{y}}^H\} = \mathbf{U}\mathbf{\Lambda}\mathbf{U}^H$  where  $\mathbf{\Lambda} = \text{diag}\{\lambda_i\}_{i=0}^3$  and by the fixed component  $\bar{\mathbf{y}}$  [20]. Specifically, defining

$$\mathbf{d} = [d_0 \ d_1 \ d_2 \ d_3]^T = \text{diag} \left\{ \frac{1}{\sqrt{\lambda_0}}, \dots, \frac{1}{\sqrt{\lambda_r(\mathbf{C}_{\tilde{\mathbf{y}}})^{-1}}}, 0, \dots, 0 \right\} \mathbf{U}^H \bar{\mathbf{y}},$$

we get

$$P(\hat{s}_i \neq s_i) \leq \bar{N}_e e^{-\frac{E_s d_{min}^2}{4\sigma_n^2} \|\bar{\mathbf{y}}\|^2} \prod_{i=0}^{r(\mathbf{C}_{\tilde{\mathbf{y}}})-1} e^{\frac{\left(\frac{E_s d_{min}^2}{4\sigma_n^2} |d_i| \lambda_i\right)^2}{1 + \frac{E_s d_{min}^2}{4\sigma_n^2} \lambda_i}}, \quad (8)$$

where  $P(\hat{s}_i \neq s_i) = \mathcal{E}_{\mathbf{H}}\{P(\hat{s}_i \neq s_i | \mathbf{H})\}$  is the probability of symbol error averaged over all channel realizations. We note that (8) correctly reflects the trends of the actual symbol error rate for varying channel statistics (see Sec. V, Simulation Examples 5, 6, and 7 ). However, these expressions may not serve as accurate estimates of the average symbol error rate  $\bar{P}_{div}$ . This limitation may be overcome by scaling (8) by an empirically determined constant  $k$  which is obtained by fitting the function  $ke^{-\frac{x^2}{2}}$  to  $Q(x)$  in a least squares sense, over the desired range of SNR.

Unlike SM, averaging over vector error events is not required to calculate the symbol error rate for the Alamouti scheme. This is due to simplification of the vector detection problem into independent scalar detection problems, as mentioned earlier. One might argue that the nearest

<sup>7</sup>For an  $m \times n$  matrix  $\mathbf{A} = [\mathbf{a}_0 \ \mathbf{a}_1 \ \dots \ \mathbf{a}_{n-1}]$ ,  $\text{vec}(\mathbf{A}) = [\mathbf{a}_0^T \ \mathbf{a}_1^T \ \dots \ \mathbf{a}_{n-1}^T]^T$  is a vector of dimension  $mn \times 1$ .

neighbor based approach that is used to determine symbol error rate for scalar constellations could be extended to vector constellations and used for SM. However, a matrix channel preserves the relative geometry of the elements of a vector constellation only if every realization of the channel is orthogonal (i.e.  $\mathbf{H}\mathbf{H}^H = \eta\mathbf{I}_2$ , where  $\eta > 0$ ), which is definitely not the case in practice. Thus, the calculation of nearest neighbors is channel dependent and hence very tedious. It is for this reason that we resorted to the weighted average pairwise error probability approach for SM.

We note that in some special cases (8) may be used to study the effect of polarization diversity and fading signal correlation on the Alamouti scheme analytically. Consider the case of pure Rayleigh fading where  $K = 0$ . We would like to identify channel characteristics that minimize the uncoded average symbol error rate  $\bar{P}_{div}$ . Minimizing  $\bar{P}_{div}$  is equivalent to maximizing  $\prod_{i=0}^r (\mathbf{C}_{\tilde{\mathbf{y}}})^{-1} \left(1 + \frac{E_s d_{min}^2}{4\sigma_n^2} \lambda_i\right)$ . Restricting our attention to full rank  $\mathbf{C}_{\tilde{\mathbf{y}}}$ , we observe that since the logarithm is a strictly monotonic function we can equivalently express the objective function for the maximization as

$$\max_{\lambda_i} \sum_{i=0}^3 \log \left(1 + \frac{E_s d_{min}^2}{4\sigma_n^2} \lambda_i\right). \quad (9)$$

Performing the maximization in (9) under the constraint of fixed total average channel power which is equivalent to constraining  $\text{Tr}(\mathbf{C}_{\tilde{\mathbf{y}}})$  to be constant, it is easily seen that (9) is maximized when all the eigenvalues  $\lambda_i$  ( $i = 0, 1, 2, 3$ ) are equal. Equivalently,  $\mathbf{C}_{\tilde{\mathbf{y}}}$  must be an orthogonal matrix to achieve minimum symbol error rate under a total average channel power constraint. For our channel model, we get

$$\mathbf{C}_{\tilde{\mathbf{y}}} = \begin{bmatrix} 1 & r\sqrt{\alpha} & t\sqrt{\alpha} & 0 \\ r^*\sqrt{\alpha} & \alpha & 0 & t\sqrt{\alpha} \\ t^*\sqrt{\alpha} & 0 & \alpha & r\sqrt{\alpha} \\ 0 & t^*\sqrt{\alpha} & r^*\sqrt{\alpha} & 1 \end{bmatrix}. \quad (10)$$

It is now easy to verify that  $\mathbf{C}_{\tilde{\mathbf{y}}}$  is orthogonal if and only if  $t = r = 0$  and  $\alpha = 1$ . Thus, under a total average channel power constraint,  $\bar{P}_{div}$  is minimized for spatially uncorrelated fading and in the absence of polarization diversity (i.e.  $\alpha = 1$  or equivalently two uni-polarized antennas rather than one dual-polarized antenna should be used), which corresponds to the classical i.i.d. Rayleigh fading MIMO channel model. Presence of fading signal correlation and/or the use of dual-polarized antennas necessarily lead to a performance loss. Now consider a situation where fading signal correlation is present, i.e.,  $r > 0$  or  $t > 0$ . For high SNR, maximizing

$\prod_{i=0}^3 \left(1 + \frac{E_s d_{min}^2}{4\sigma_n^2} \lambda_i\right)$  is equivalent to maximizing<sup>8</sup>  $\det(\mathbf{C}_{\tilde{\mathbf{y}}})$ . Straightforward manipulations reveal that

$$\mathbf{C}_{\tilde{\mathbf{y}}} = \begin{bmatrix} 1 & 0 & 0 & 0 \\ 0 & \sqrt{\alpha} & 0 & 0 \\ 0 & 0 & \sqrt{\alpha} & 0 \\ 0 & 0 & 0 & 1 \end{bmatrix} \begin{bmatrix} 1 & r & t & 0 \\ r^* & 1 & 0 & t \\ t^* & 0 & 1 & r \\ 0 & t^* & r^* & 1 \end{bmatrix} \begin{bmatrix} 1 & 0 & 0 & 0 \\ 0 & \sqrt{\alpha} & 0 & 0 \\ 0 & 0 & \sqrt{\alpha} & 0 \\ 0 & 0 & 0 & 1 \end{bmatrix}.$$

Using the identity  $\det(\mathbf{AB}) = \det(\mathbf{A})\det(\mathbf{B})$ , it is easily seen that for given fading signal correlation, the symbol error rate estimate is minimized when  $\alpha$  is maximum, or equivalently,  $\alpha = 1$ . Thus, even in the presence of fading signal correlation, polarization diversity leads to a performance loss of the Alamouti scheme at high SNR. Simulation Examples 2 and 3 in Sec. V will show that this is in general not the case for SM.

We conclude this section by noting that for the Alamouti scheme the use of polarization diversity always leads to a performance loss and that transmit and receive correlation have symmetric effects on the symbol error rate. The latter statement is easily verified through an analysis of the eigenvalues of  $\mathbf{C}_{\tilde{\mathbf{y}}}$  in (10).

## V. SIMULATION RESULTS

In this section, we provide simulation results demonstrating the performance of SM and the Alamouti scheme for varying channel statistics. We simulated a system with 1 dual-polarized transmit and 1 dual-polarized receive antenna. In order to keep the data rates in both systems the same, the data symbols for SM were drawn from a 4-QAM constellation while the data symbols for the Alamouti scheme were drawn from a 16-QAM constellation. ML decoding with perfect channel knowledge was performed. The SNR was defined as  $\text{SNR} = 10 \log_{10} \frac{2E_s}{\sigma_n^2}$  (dB). Unless otherwise specified, the fixed component of the channel was chosen as  $\overline{\mathbf{H}} = \begin{bmatrix} 1 & \sqrt{\alpha_f} \\ \sqrt{\alpha_f} & 1 \end{bmatrix}$ . All simulation results were obtained by averaging over  $1.5 \times 10^5$  independent Monte Carlo trials.

**Simulation Example 1.** The first simulation example serves to demonstrate that  $\bar{P}_{mux}$  provides an accurate estimate of the symbol error rate for SM. For  $t = 0.5$ ,  $r = 0.3$ ,  $\alpha = 0.4$ , and  $\alpha_f = 0.3$ , Fig. 4 shows the symbol error rate obtained using Monte Carlo simulations along with the estimated symbol error rate,  $\bar{P}_{mux}$ , for  $K = 0$  and  $K = 10$ . It can be seen that especially in the high SNR regime ( $\text{SNR} \geq 8$  dB) the symbol error rate estimate  $\bar{P}_{mux}$  closely matches

<sup>8</sup> $\det(\mathbf{A})$  stands for the determinant of the matrix  $\mathbf{A}$ .

the actual symbol error rate. Note, however, that  $\bar{P}_{mux}$  is neither a strict upper- nor a strict lower-bound on the symbol error rate.

**Simulation Example 2.** The second simulation example demonstrates the benefit of polarization diversity under pure Rayleigh fading conditions for SM. For an SNR of 15 dB, Fig. 5 shows the symbol error rate along with  $\bar{P}_{mux}$  as a function of  $\alpha$  for various values of  $t$  and for  $r = 0$ . Noting that  $\alpha = 1$  can be interpreted as having two uni-polarized antennas on each side of the link all of which employ the same polarization, we can draw the following conclusions. If the transmitter can not afford large antenna spacing and/or scattering in the channel is not rich enough and hence the use of two physical antennas results in high transmit antenna correlation, it is always better to use one dual-polarized antenna even if the two polarizations are highly correlated. In practice, however, the use of dual-polarized antenna elements will reduce transmit correlation so that the improvement over the case of two physical antennas will be even more pronounced. In fact, if the transmit correlation is very high, it follows from Fig. 5 that the use of SM is not possible any more (due to the high error rates), whereas replacing the two antennas by a dual-polarized antenna with small  $\alpha$  yields error rates that are acceptable. In fact, the use of polarization diversity can improve the average uncoded symbol error rate by up to an order of magnitude. We can furthermore conclude from Fig. 5 that if the transmitter can afford large antenna spacings and/or scattering in the channel is rich enough, the use of dual-polarized antennas will always result in a performance loss. The physical interpretation of these results is as follows. When the transmit correlation starts to increase and hence the condition number of the channel matrix realizations increases or equivalently the angle between the realizations of the two columns decreases, polarization diversity yields improved spatial separation and hence increases the multiplexing gain. More specifically, consider the case of  $t = 1$ . In the absence of polarization diversity ( $\alpha = 1$ ) vector error events such as  $[d_{min} - d_{min}]^T$  lie in the null-space of the channel, resulting in a high error rate. This effect subsides with the introduction of polarization diversity and good XPD. Through simulations, we found that starting at  $t = 0.85$ , polarization diversity, i.e.,  $\alpha < 1$ , starts improving the multiplexing gain.

**Simulation Example 3.** In this simulation example, we study the performance of SM with polarization diversity in the presence of receive correlation only. For an SNR of 15 dB and  $K = 0$ , Fig. 6 shows the symbol error rate along with the estimate  $\bar{P}_{mux}$  for  $t = 0$  and various values of  $r$ . We observe that for high receive correlation the use of polarization diversity can

lead to a slight improvement in terms of symbol error rate. This effect, however, is much less pronounced than in the case of transmit correlation only. The asymmetry in the impact of polarization diversity in the cases of transmit correlation only and receive correlation only for SM has been noted in Sec. III. The reason for the pronounced difference is that in the presence of high transmit correlation only the use of polarization diversity improves the spatial separation of the two independent data streams which does not happen in the case of receive correlation only. A more detailed description of this observation is provided in [22]. To summarize, in the presence of receive correlation only the use of dual-polarized antennas is generally not advised.

**Simulation Example 4.** This simulation example shows the potential benefit of dual-polarized antennas at high K-factor for systems employing SM. For high K-factor, the symbol error rate is governed primarily by the characteristics of the fixed component  $\overline{\mathbf{H}}$ . In Fig. 7, we plot the symbol error rate as a function of  $\alpha_f$  for  $t = 0.5, r = 0.3, \alpha = 0.4, K = 10$  and an SNR of 15 dB. Again noting that  $\alpha_f = 1$  corresponds to the case of two physical uni-polarized antennas, the plot reveals that system performance improves by over an order of magnitude with the use of dual-polarized antennas. Similar to Simulation Example 2, when XPD for the fixed component is poor, there are vector error events which tend to excite the null-space of the channel matrix in the presence of high K-factor, leading to a high symbol error rate. The use of dual-polarized antennas mitigates this problem. We would like to note that this conclusion is a consequence of our choice of channel model, namely a rank deficient  $\overline{\mathbf{H}}$  for  $\alpha_f = 1$ . This model has been verified through measurements in [25] and reflects the fact that the use of polarization diversity improves spatial separation.

The improvement in performance that polarization diversity offers with increasing K-factor can also be analyzed from the point of view of channel capacity [26], [27]. At high K-factor, in the absence of polarization diversity ( $\alpha_f = 1$ ), the channel  $\mathbf{H}$  tends to be ill-conditioned. Hence, only one significant spatial sub-channel is present between transmitter and receiver. With the introduction of polarization diversity ( $\alpha_f < 1$ ) the rank of the channel is restored and two significant spatial data pipes are available between transmitter and receiver resulting in multiplexing gain.

**Simulation Example 5.** This example serves to demonstrate that  $\overline{P}_{div}$  provides an accurate estimate of the symbol error rate for the Alamouti scheme. For  $t = 0.7, r = 0.1, \alpha = 0.2, \alpha_f = 0.6$  and scaling constant  $k = 0.25$ , Fig. 8 shows the symbol error rate obtained using Monte Carlo

simulations along with the estimated symbol error rate  $\bar{P}_{div}$  for  $K = 0$  and  $K = 10$ . It can be seen that the symbol error rate estimate closely matches the actual symbol error rate (even for small SNR values).

**Simulation Example 6.** In this example, we demonstrate that the use of polarization diversity in the context of TD employing the Alamouti scheme leads to a performance loss. We furthermore show the symmetric impact of transmit and receive correlation on the Alamouti scheme’s error rate performance. (Recall that in the case of SM this impact is asymmetric). Fig. 9 depicts the symbol error rate as a function of  $\alpha$  for  $K = 0$  and SNR = 17 dB (left plot shows  $t = 0$  and various values of  $r$ , right plot shows  $r = 0$  and various values of  $t$ ). It is clearly seen that  $\alpha = 1$  results in the lowest symbol error rate for all scenarios. This corroborates the observation made towards the end of Sec. IV. Moreover, we can see that transmit and receive correlation have an identical impact on the performance of the Alamouti scheme (as opposed to SM), as mentioned in the last paragraph of Sec. IV. Additionally, Fig. 9 shows how the performance of the Alamouti scheme degrades with increasing fading signal correlation.

**Simulation Example 7.** In the last simulation example, we investigate the influence of K-factor on the Alamouti scheme. We consider a channel with  $\alpha = \alpha_f$ . This corresponds to a situation where  $\|\overline{\mathbf{H}}\|_F^2 = \mathcal{E}\{\|\widetilde{\mathbf{H}}\|_F^2\}$ . As described in Simulation Example 4, at high K-factor,  $\overline{\mathbf{H}}$  governs the behavior of the system, while  $\widetilde{\mathbf{H}}$  dominates at low K-factor. Fig. 10 shows the symbol error rate for the Alamouti scheme as a function of  $K$  for  $t = 0.5, r = 0.3$ , and  $\alpha = \alpha_f = 0.6$  for an SNR of 17 dB. It is clear from Fig. 10 that system performance improves with increasing K-factor. This conforms with intuition – at high K-factor, the system “looks more like an AWGN link” and outperforms a fading channel with the same average channel power. This result does not extend to SM, where system performance at high K-factor is primarily a function of the geometry of  $\overline{\mathbf{H}}$  relative to the geometry of the transmitted vector constellation. If the geometry of  $\overline{\mathbf{H}}$  is not conducive (in the uncoded case typically when the condition number of  $\overline{\mathbf{H}}$  is high), then high K-factor will result in a significant performance loss in the case of SM.

## VI. CONCLUSIONS

We studied the use of dual-polarized antennas for spatial multiplexing and the Alamouti scheme. While dual-polarized antennas typically yield a performance degradation for the Alamouti scheme, they can be quite beneficial to spatial multiplexing under a wide variety of channel conditions, some of which we have highlighted in the paper. For instance, for pure Rayleigh fading

ing, and in the presence of high transmit fading signal correlation *dual-polarized antennas* can yield *significantly improved multiplexing gain*. Also, for high K-factor the use of dual-polarized antennas was found to be generally highly beneficial for spatial multiplexing. We proposed new techniques to estimate the uncoded average symbol error rates for spatial multiplexing and the Alamouti scheme. These techniques allow a numerical (and often also analytical) study of the impact of polarization diversity on the performance of spatial multiplexing and the Alamouti scheme for arbitrary channel statistics. We verified the accuracy of our symbol error rate estimates through comparison with numerical results and studied the impact of varying channel conditions on the performance of the two transmission strategies. The proposed techniques reveal all trends of the actual symbol error rate for varying channel characteristics correctly without having to resort to time-consuming computer simulations and provide insight into channel suitability for each of these schemes.

#### ACKNOWLEDGMENTS

R. U. Nabar's work was supported by the Dr. T. J. Rodgers Stanford Graduate Fellowship. The work of H. Bölcskei was supported by FWF grant J1868-TEC and by NSF grants CCR 99-79381 and ITR 00-85929.

#### REFERENCES

- [1] A. J. Paulraj and T. Kailath, "Increasing capacity in wireless broadcast systems using distributed transmission/directional reception," *U. S. Patent*, no. 5,345,599, 1994.
- [2] G. J. Foschini, "Layered space-time architecture for wireless communication in a fading environment when using multi-element antennas," *Bell Labs Tech. J.*, pp. 41–59, Autumn 1996.
- [3] I. E. Telatar, "Capacity of multi-antenna Gaussian channels," *European Trans. Tel.*, vol. 10, no. 6, pp. 585–595, Nov./Dec. 1999.
- [4] G. G. Raleigh and J. M. Cioffi, "Spatio-temporal coding for wireless communication," *IEEE Trans. Comm.*, vol. 46, no. 3, pp. 357–366, March 1998.
- [5] H. Bölcskei, D. Gesbert, and A. J. Paulraj, "On the capacity of OFDM-based spatial multiplexing systems," *IEEE Trans. Comm.*, vol. 50, no. 2, pp. 225–234, Feb. 2002.
- [6] N. Seshadri and J. Winters, "Two signaling schemes for improving the error performance of frequency-division-duplex (FDD) transmission systems using transmitter antenna diversity," *Int. J. Wireless Information Networks*, vol. 1, no. 1, pp. 49–60, Jan. 1994.
- [7] J. Guey, M. Fitz, M. Bell, and W. Kuo, "Signal design for transmitter diversity wireless communication systems over Rayleigh fading channels," in *Proc. IEEE VTC*, Atlanta, GA, April/May 1996, vol. 1, pp. 136–140.

- [8] V. Tarokh, N. Seshadri, and A. R. Calderbank, "Space-time codes for high data rate wireless communication: Performance criterion and code construction," *IEEE Trans. Inf. Theory*, vol. 44, no. 2, pp. 744–765, March 1998.
- [9] V. Tarokh, H. Jafarkhani, and A.R. Calderbank, "Space-time block codes from orthogonal designs," *IEEE Trans. Inf. Theory*, vol. 45, no. 5, pp. 1456–1467, July 1999.
- [10] S. M. Alamouti, "A simple transmit diversity technique for wireless communications," *IEEE J. Sel. Areas Comm.*, vol. 16, no. 8, pp. 1451–1458, Oct. 1998.
- [11] H. Bölcskei, R. U. Nabar, V. Erceg, D. Gesbert, and A. J. Paulraj, "Performance of spatial multiplexing in the presence of polarization diversity," in *Proc. IEEE ICASSP*, Salt Lake City, UT, May 2001, vol. 4, pp. 2437–2440.
- [12] R. U. Nabar, V. Erceg, H. Bölcskei, and A. J. Paulraj, "Performance of multi-antenna signaling strategies using dual-polarized antennas: Measurement results and analysis," in *Proc. IEEE WPMC*, Aalborg, Denmark, Sept. 2001, vol. 1, pp. 175–180.
- [13] D. S. Baum, D. A. Gore, R. U. Nabar, S. Panchanathan, K. V. S. Hari, V. Erceg, and A. J. Paulraj, "Measurement and characterization of broadband MIMO fixed wireless channels at 2.5 GHz," in *Proc. IEEE Int. Conf. on Personal Wireless Comm.*, Hyderabad, India, Dec. 2000, pp. 203–206.
- [14] G. L. Stüber, *Principles of Mobile Communication*, Kluwer Academic Publishers, Norwell, MA, 1996.
- [15] T. Neubauer and P. C. F. Eggers, "Simultaneous characterization of polarization diversity matrix components in pico cells," in *Proc. IEEE VTC - Fall*, Amsterdam, The Netherlands, 1999, vol. 3, pp. 1361–1365.
- [16] J. J. A. Lempiäinen and J. K. Laiho-Steffens, "The performance of polarization diversity schemes at a base station in small/micro cells at 1800 MHz," *IEEE Trans. Veh. Tech.*, vol. 47, no. 3, pp. 1087–1092, Aug. 1998.
- [17] R. G. Vaughan, "Polarization diversity in mobile communications," *IEEE Trans. Veh. Tech.*, vol. 39, no. 3, pp. 177–186, Aug. 1990.
- [18] P. C. F. Eggers, J. Tøftgård, and A. M. Oprea, "Antenna systems for base station diversity in urban small and micro cells," *IEEE J. Sel. Areas Comm.*, vol. 11, no. 7, pp. 1046–1057, Sept. 1993.
- [19] J. G. Proakis, *Digital Communications*, McGraw-Hill, New York, 3rd edition, 1995.
- [20] R. U. Nabar, H. Bölcskei, and A. J. Paulraj, "Outage performance of space-time block codes for generalized MIMO channels," *IEEE Trans. Inf. Theory*, March 2002, submitted.
- [21] M. P. Fitz, J. Grimm, and S. Siwamogsatham, "A new view of performance analysis techniques in correlated Rayleigh fading," in *Proc. IEEE WCNC*, New Orleans, LA, Sept. 1999, vol. 1, pp. 139–144.
- [22] H. Bölcskei and A. J. Paulraj, "Performance analysis of space-time codes in correlated Rayleigh fading environments," in *Proc. of Asilomar Conf. on Signals, Systems, and Computers*, Pacific Grove, CA, Nov. 2000, vol. 1, pp. 687–693.
- [23] M. Uysal and C. N. Georghiades, "Effect of spatial fading correlation on performance of space-time codes," *Electronics Letters*, vol. 37, no. 3, pp. 181–183, Feb. 2001.
- [24] J. M. Cioffi, *Class Reader for EE379a – Digital Communication: Signal Processing*, Stanford University, Stanford, CA. Available online at <http://www.stanford.edu/class/ee379a>.
- [25] V. Erceg, P. Soma, D. S. Baum, and A. J. Paulraj, "Capacity obtained from multiple-input multiple-output

- channel measurements in fixed wireless environments at 2.5 GHz,” in *Proc. IEEE ICC*, New York, NY, April/May 2002, vol. 1, pp. 396–400.
- [26] M. Godavarti, A. O. Hero, and T. L. Marzetta, “Min-capacity of a multiple antenna wireless channel in a static Rician fading environment,” in *Proc. IEEE ISIT*, Washington, DC, June 2001, p. 57.
- [27] M. Godavarti, T. L. Marzetta, and S. Shamai, “Capacity of a mobile multiple-antenna wireless link with isotropically random Rician fading,” in *Proc. IEEE ISIT*, Washington, DC, June 2001, p. 323.

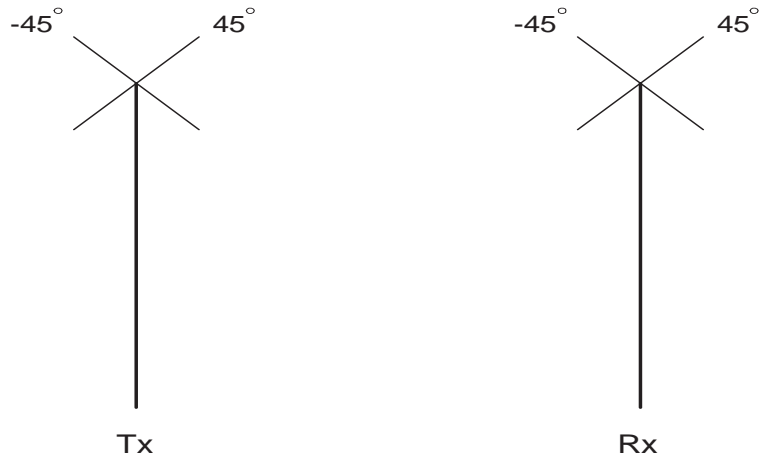


Fig. 1.

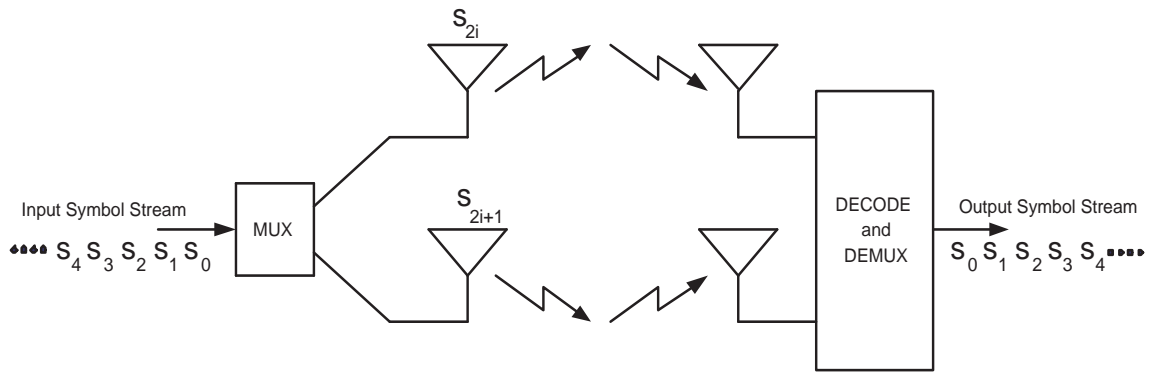


Fig. 2.

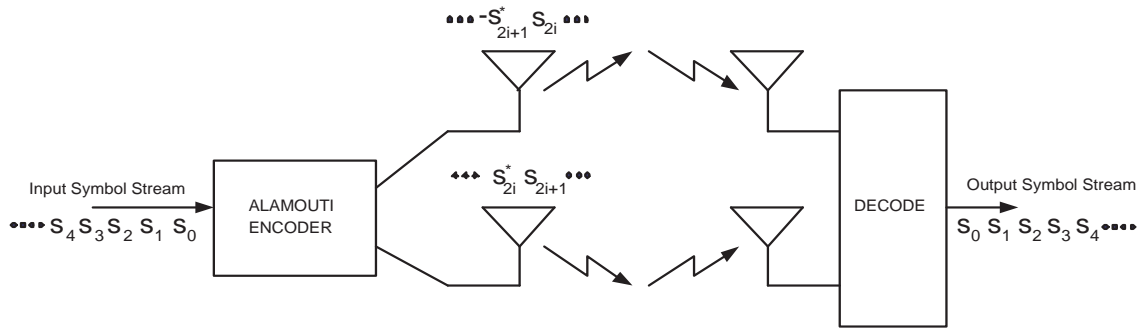


Fig. 3.

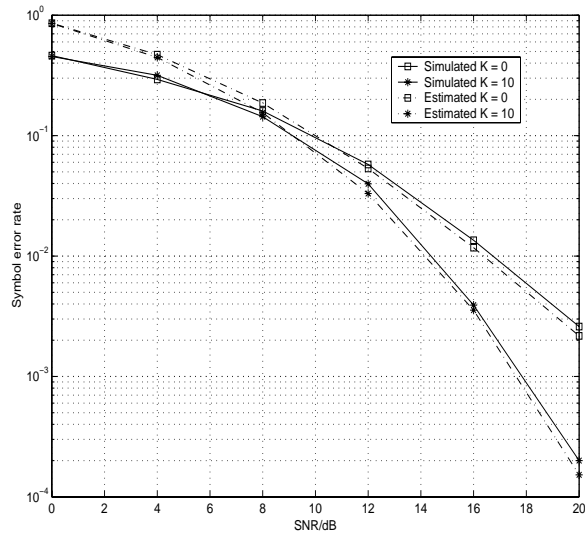


Fig. 4.

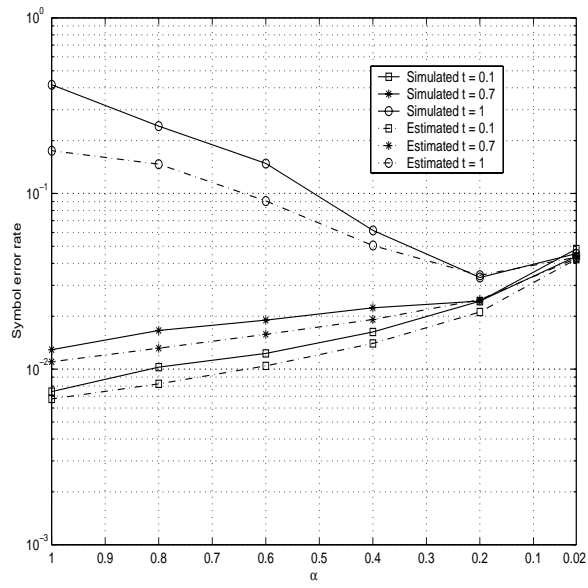


Fig. 5.

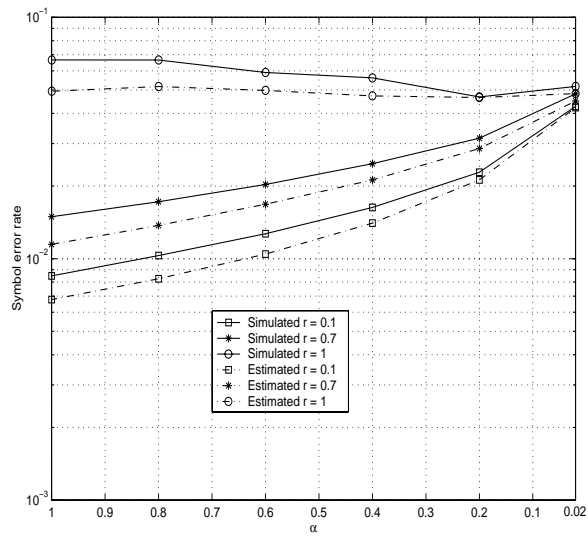


Fig. 6.

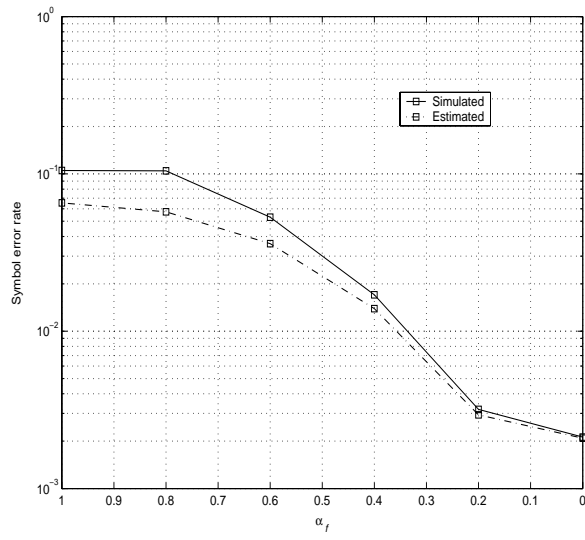


Fig. 7.

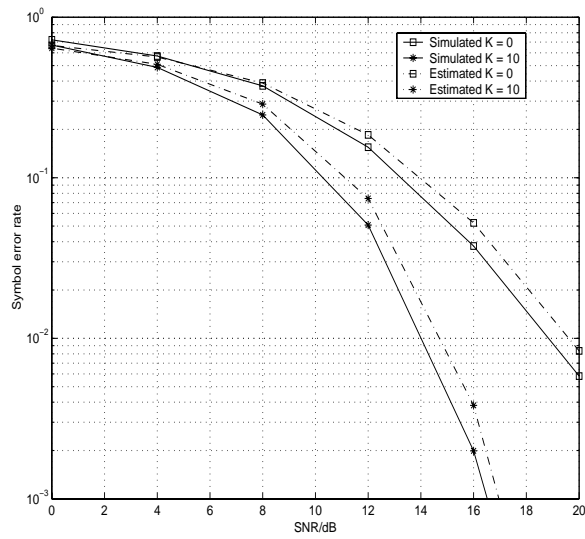


Fig. 8.

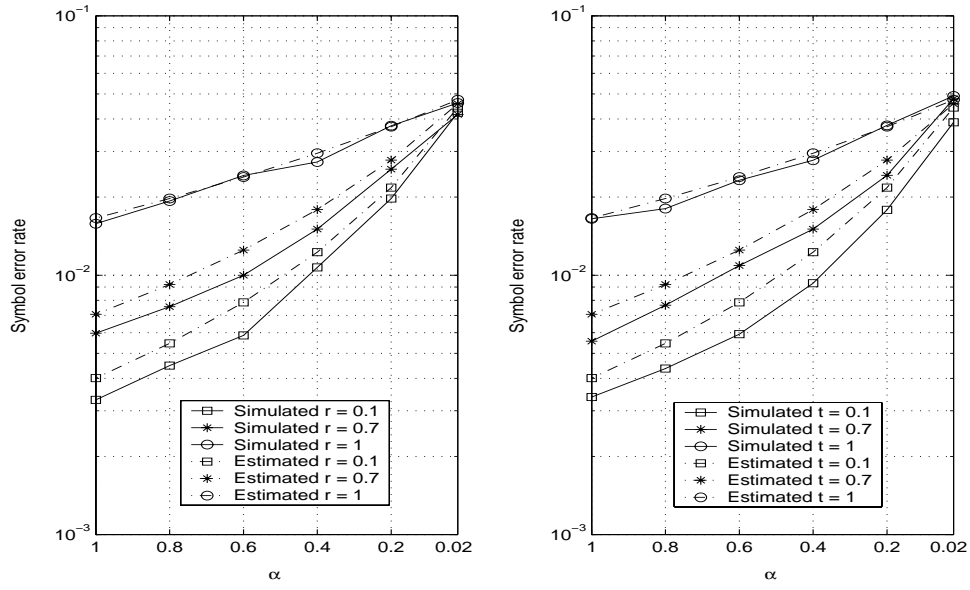


Fig. 9.

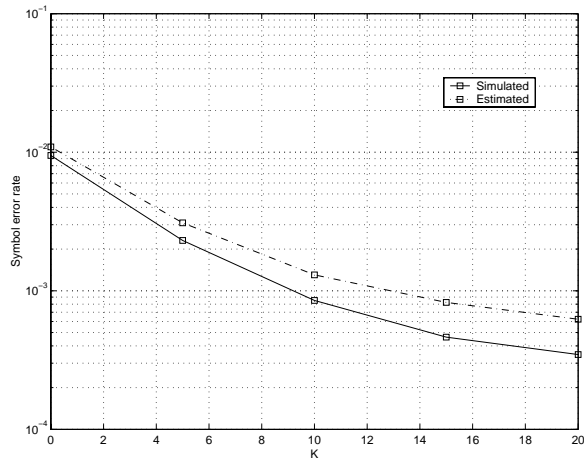


Fig. 10.

## Figure Captions

*Fig. 1 Schematic of a dual-polarized  $+45^\circ / -45^\circ$  antenna setup.*

*Fig. 2 Schematic of a spatial multiplexing system.*

*Fig. 3 Schematic of the Alamouti scheme.*

*Fig. 4 Symbol error rate for spatial multiplexing as a function of SNR for varying  $K$ -factor. For high SNR, the estimate closely matches the actual symbol error rate.*

*Fig. 5 Symbol error rate for spatial multiplexing as a function of  $\alpha$  for various values of transmit correlation  $t$ . The use of polarization diversity can yield significant improvements in terms of symbol error rate if the transmit correlation is high.*

*Fig. 6 Symbol error rate for spatial multiplexing as a function of  $\alpha$  for various values of receive correlation  $r$ . The use of polarization diversity in the presence of receive correlation only is generally not advised.*

*Fig. 7 Symbol error rate for spatial multiplexing as a function of  $\alpha_f$ . For high  $K$ -factor, the use of polarization diversity can yield significant improvements in terms of symbol error rate.*

*Fig. 8 Symbol error rate for the Alamouti scheme as a function of SNR for varying  $K$ -factor. The estimate closely matches the actual symbol error rate (even for small SNR values).*

*Fig. 9 Symbol error rate for the Alamouti scheme as a function of  $\alpha$  for varying receive or transmit correlation. The use of dual-polarized antennas leads to a performance loss.*

*Fig. 10 Symbol error rate for the Alamouti scheme as a function of  $K$ -factor. The performance improves with increasing  $K$ -factor.*

## Biographies

**Rohit U. Nabar** was born in Bombay, India on Dec. 18, 1976. He received the B.S. (*summa cum laude*) degree in electrical engineering from Cornell University, Ithaca, NY in 1998 and the M.S. degree in electrical engineering from Stanford University, Stanford, CA in 2000. He is currently a doctoral student in the Smart Antennas Research Group at Stanford University and is the recipient of the Dr. T. J. Rodgers Stanford Graduate Fellowship. His research interests are in the areas of signal processing for wireless communications and multi-input multi-output (MIMO) antenna systems.

**Helmut Bölcskei** (M'98) was born in Mödling, Austria on May 29, 1970. He received the Dipl.-Ing. and Dr. techn. degrees in electrical engineering/communications from Vienna University of Technology, Vienna, Austria, in 1994 and 1997, respectively.

From 1994 to 2001 he was with the Institute of Communications and Radio-Frequency Engineering, Vienna University of Technology. From March 2001 to January 2002, he was an Assistant Professor of Electrical Engineering at the University of Illinois at Urbana-Champaign. Since February 2002 he has been an Assistant Professor of Communication Theory at ETH Zurich. He was a visiting researcher at Philips Research Laboratories Eindhoven, The Netherlands, ENST Paris, France, and the Heinrich-Hertz-Institute Berlin, Germany. From February 1999 to February 2001 he was a postdoctoral researcher in the Smart Antennas Research Group in the Information Systems Laboratory, Department of Electrical Engineering, Stanford University, Stanford, CA. From 1999-2001 he was a consultant for Iospan Wireless Inc. (formerly Gigabit Wireless Inc.).

His research interests include communication and information theory and statistical signal processing with special emphasis on wireless communications, multi-input multi-output (MIMO) antenna systems, space-time coding, Orthogonal Frequency Division Multiplexing (OFDM), and wireless networking.

He received a 2001 IEEE Signal Processing Society Young Author Best Paper Award and was an Erwin Schrödinger Fellow (1999-2001) of the Austrian National Science Foundation (FWF). He serves as an associate editor for the IEEE Transactions on Wireless Communications and the IEEE Transactions on Signal Processing.

**Vinko Erceg** received the B.S.E.E. in 1988 and the Ph.D.E.E. in 1992, both from the City University of New York. From 1990 to 1992, he was a Lecturer at the Electrical Engineering Department at the City College of NY, concurrently working with SCS Mobilecom, Port Washington, NY, on spread-spectrum systems for mobile communications. In 1992, he joined AT&T Bell Laboratories and became a Principal Member of Technical Staff in the Wireless Communications Research Department of AT&T Labs-Research in 1996. He participated in various aspects of wireless research, including signal propagation modeling, communication systems engineering and performance analysis. He joined Iospan Wireless Inc., San Jose, CA, in February 2000, where he now serves as Director and Principal Engineer in Channel Modeling and Systems Validation. In 2001, he chaired the IEEE 802.16 working group on broadband wireless access standards in developing NLOS channel models. His research interests include radio propagation, capacity, performance, and coverage prediction of cellular and MIMO wireless systems.

**David Gesbert** holds a Ph.D degree from Ecole Nationale Supérieure des Telecommunications (ENST), Paris, France, 1997. From 1993 to 1997, he was with France Telecom Research (CNET), Radio Systems Department, Paris. From April 1997 to October 1998, he was a postdoctoral fellow in the Information Systems Laboratory, Stanford University. In October 1998, he took part in the founding team of Iospan Wireless Inc. (formerly Gigabit Wireless Inc.), San Jose, CA, a startup company promoting high-speed wireless internet access networks using adaptive MIMO, OFDM, and other state-of-the-art applied wireless research. In 2001, he became an independent consultant and joined in parallel the Signal Processing Group, Department of Informatics, at the University of Oslo, Norway, as an Adjunct Associate Professor. Dr. Gesbert is the author of over 40 papers and 15 patents, granted or pending, in the area of wireless systems. His research interests are in the area of high-speed wireless data/IP networks, smart antennas and MIMO, link layer and system optimization.

**Arogyaswami J. Paulraj** has been a Professor at the Department of Electrical Engineering, Stanford University since 1993, where he supervises the Smart Antennas Research Group. This group consists of approximately a dozen researchers working on applications of space-time signal processing for wireless communications networks. His research group has developed many key fundamentals of this new field and helped shape a worldwide research and development focus

on this technology.

Paulraj was educated at the Naval Engineering College and the Indian Institute of Technology, India (Ph.D. 1973). His non-academic positions included Head, Sonar Division, Naval Oceanographic Laboratory, Cochin; Director, Center for Artificial Intelligence and Robotics, Bangalore; Director, Center for Development of Advanced Computing; Chief Scientist, Bharat Electronics, Bangalore, and Chief Technical Officer and Founder, Iospan Wireless Inc.. He has also held visiting appointments at Indian Institute of Technology, Delhi, Loughborough University of Technology, and Stanford University. Paulraj sits on several board of directors and advisory boards for US and Indian companies/venture partnerships.

Paulraj's research has spanned several disciplines, emphasizing estimation theory, sensor signal processing, parallel computer architectures/algorithms and space-time wireless communications. His engineering experience includes development of sonar systems, massively parallel computers, and more recently broadband wireless systems.

Paulraj has won several awards for his engineering and research contributions. These include two President of India Medals, CNS Medal, Jain Medal, Dist. Service Medal, Most Dist. Service Medal, VASVIK Medal, IEEE Best Paper Award (Joint), amongst others. He is the author of over 250 research papers and holds eight patents. Paulraj is a Fellow of the Institute of Electrical and Electronics Engineers (IEEE) and a Member of the Indian National Academy of Engineering.